Available online at www.sciencedirect.com
SCIENCE DIRECT®
ELSEVIER
International Journal of Solids and Structures 41 (2004) 6111–6127
INTERNATIONAL JOURNAL OF SOLIDS and STRUCTURES
www.elsevier.com/locate/ijsolstr

Surface energy effects for cavity growth and nucleation in an incompressible neo-Hookean material—modeling and experiment

J. Dollhofer [a,1], A. Chiche [a], V. Muralidharan [b], C. Creton [a,*], C.Y. Hui [b]

[a] *Laboratoire Physique et Chimie Structurale et Macromoléculaire à l'Ecole Supérieure de Chimie et Physique Industrielles, 10, Rue Vauquelin, 75005 Paris, France*

[b] *Department of Theoretical and Applied Mechanics, Cornell University, Ithaca, NY 14853, USA*

Received 29 April 2004
Available online 24 June 2004

Abstract

The effect of surface tension γ on cavity nucleation and growth in an incompressible neo-Hookean material of initial elasticity modulus E is examined. In a numerical analysis of potential energy limited to spherically symmetric configurations, a bifurcation problem is identified. If the applied uniform radial tensile dead-load is sufficiently large, a branch corresponding to cavity expansion bifurcates from the branch corresponding to cavity constriction due to surface tension. The bifurcation is interpreted in terms of a sudden growth to a finite cavity radius which bears some reminiscence of the snap-through buckling phenomenon in structural mechanics. The finding is compared to experimental results obtained in probe tack tests of soft adhesives where rapid cavity growth is also observed. Some of the experimental evidence is explained by assuming that in the adhesive there is a distribution of pre-existing cavities whose radius compares in a way to the length scale γ/E such as to make them susceptible to the influence of surface tension.

Keywords: Cavitation; Sudden cavity growth; Finite-strain elasticity; Surface tension; Pressure sensitive adhesives

1. Introduction and review

The formation of cavities in a nearly incompressible hyperelastic material is a problem of technological relevance in many areas of materials science. Typically, cavitation occurs when an elastomer is mechanically loaded with a hydrostatic negative pressure without any possibility to relax that stress through shear deformation. This situation is encountered for example when a rubber film is sandwiched between two harder layers which are pushed apart. While the theoretical treatment of the expansion of a cavity in such a

* Corresponding author. Tel.: +33-1-40-79-46-83; fax: +33-1-40-79-46-86.
E-mail address: costantino.creton@espci.fr (C. Creton).
[1] Current address: Valeo Lighting Systems, 93012 Bobigny/Paris, France.

0020-7683/$ - see front matter © 2004 Elsevier Ltd. All rights reserved.
doi:10.1016/j.ijsolstr.2004.04.041

material has been the focus of numerous publications, it has proved more difficult to gather direct experimental evidence on how the process of cavity growth is triggered, rendering direct comparisons between theory and experiment relatively rare. However recently, new measurements that could be tested against existing theories have become available stemming from the careful study of the mechanisms of detachment of a self-adhesive material from a solid surface (Lakrout et al., 1999; Brown et al., 2002; Chiche et al., 2003). It has been found that when a thin confined layer of self-adhesive material is subjected to a tensile load, the primary failure mechanism is the formation of cavities above a certain threshold of tensile stress. Several new interesting experimental observations have been made, justifying a revisit of existing models for cavity expansion. In particular, it has been found that:

1. Cavities did not appear at a fixed level of hydrostatic stress but, at a range of stresses. This was attributed to the existence of defects of varying sizes. However, at a given fixed level of tensile stress, new cavities appeared slowly over time, implying a stress or temperature activated process for the expansion.
2. The distribution of stresses at which the cavities appear, was centered at a value significantly higher than the Young's modulus of the adhesive.
3. The average cavitation stress increased markedly with decreasing layer thickness (everything else being kept equal), implying a dependence of the expansion process on the boundary conditions of loading.

We felt that the last two observations had not been addressed in the existing literature, which we now briefly review. The expansion of a *pre-existing* cavity in an incompressible neo-Hookean material subjected to an external hydrostatic *traction* was studied by Green and Zerna (1954). In this classical work it is found that the Cauchy traction cannot exceed the value of $5E/6$ with E denoting the initial elasticity modulus. However, cavity expansion and nucleation imply the creation of new surface. Abeyratne and Hou (1991) considered the problem of cavity(traction-free) collapse in a class of incompressible elastic solids due to a constant external pressure. To the knowledge of the authors, the only work including the effect of surface tension on the elastic, finite deformation of a cavity is that by Gent and Tompkins (1969). They considered a cavity of size A in an infinite (outer radius $B \to \infty$) neo-Hookean medium as described in Fig. 1 where undeformed and deformed coordinates are denoted, respectively, by capital and small letters. The outer surface is subjected to a uniform traction T and the cavity is subjected to surface tension which adds an additional traction force pointing inwards and is given by (Gent and Tompkins, 1969)

$$T_i = \frac{2\gamma}{a}, \tag{1}$$

where T_i is the Cauchy traction due to surface tension pointing inwards and distributed over the internal deformed surface and a is the current cavity radius. For a neo-Hookean material, the solution is (Gent and Tompkins, 1969)

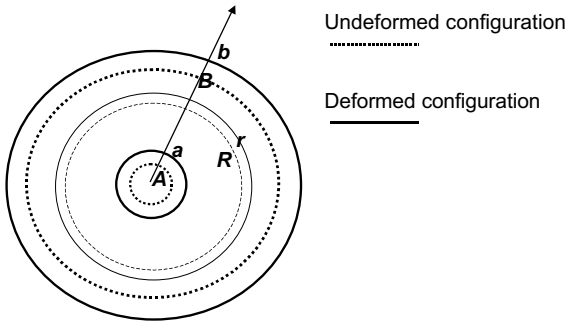

Fig. 1. Conventions for the spherical shell problem, showing the reference and current configurations.

$$T = \frac{E}{6}\left(5 - \frac{4}{\lambda} - \frac{1}{\lambda^4}\right) + \frac{2\gamma}{\lambda A}, \tag{2}$$

where γ is the surface energy per unit area and λ is the hoop stretch at the cavity surface. To clarify the role of the second term, assume that there is no external loading, $T = 0$; then (2) is

$$\frac{\lambda}{12}\left(5 - \frac{4}{\lambda} - \frac{1}{\lambda^4}\right) = -\frac{\gamma/E}{A}. \tag{3}$$

Suppose the undeformed cavity radius A is γ/E, then $\lambda \approx 0.46$, i.e. the cavity is constricted by surface tension, as expected. This example shows that the length scale

$$L_\gamma \equiv \gamma/E \tag{4}$$

corresponds to the size of a cavity which is shrunk, by surface tension, to roughly one half of its original undeformed size. It is convenient to define a normalized radius and traction by

$$\overline{A} \equiv \frac{A}{6\gamma/E} \tag{5}$$

and

$$\overline{T} = \frac{6T}{E}. \tag{6}$$

Since real tests and applications are often performed with thin films where the deformed cavities are not negligibly small when compared to the characteristic length of the specimen (Chiche et al., 2003), it is helpful to extend (2) to the case of a finite-size shell. One obtains (cf. Appendix A)

$$T = \frac{E}{6}\left(\frac{4}{\lambda_B} + \frac{1}{\lambda_B^4} - \frac{4}{\lambda} - \frac{1}{\lambda^4}\right) + \frac{2\gamma}{\lambda A}, \tag{7}$$

where λ_B is the hoop stretch at the outer surface. In normalized coordinates, (7) is

$$\overline{T} = \left(\frac{4}{\lambda_B} + \frac{1}{\lambda_B^4} - \frac{4}{\lambda} - \frac{1}{\lambda^4}\right) + \frac{2}{\lambda\overline{A}}. \tag{8}$$

Eq. (8) shows that there are two regimes: for large values of $\overline{A}$, the applied traction is dominated by the bracketed elastic energy term and one finds the classical expression of Green and Zerna (1954), while for small values of $\overline{A}$, it is the surface energy term which prevents expansion. Fig. 2 shows the relationship between the normalized true traction $\overline{T}$ and the cavity stretch λ, for a number of shells with different cavity sizes but constant material volume.

The horizontal broken line indicates the classical limiting value of $5E/6$ (Green and Zerna, 1954; Ball, 1982), the vertical broken line indicates the case when deformed and undeformed cavity radii are equal, i.e. $\lambda = 1$, and the broken curve represents the elastic response of the thick spherical shell in the absence of surface tension, (2) with $\gamma = 0$. The points indicate the maximum Cauchy traction which can be attained for a given normalized cavity radius $\overline{A}$. The first five curves indicated by the broken arrow correspond to $\overline{A} > 1$. For a neo-Hookean solid with $E = 0.05$ MPa, $\gamma = 0.03$ N/m (typical of standard pressure sensitive adhesives (PSA)), $B = 50$ μm (a reasonable value for experiments performed with thin films of soft adhesives), $\overline{A} > 1$ corresponds to $A/B > 0.072$. The last six curves indicated by the full arrow correspond to $\overline{A} < 0.01$, i.e. $A/B < 0.001$. Arrows indicate the direction of decreasing $\overline{A}$. Comparing the first set of curves to the broken curve, one recognizes that there is no cavity constriction (i.e. $\lambda \geqslant 1$). In other words, for $\overline{A} > 1$ surface tension does not substantially affect the elastic response of the shell. Rather, it is the finite thickness of these shells that introduces a variation. As is well known, for finite shells the maximum true traction is

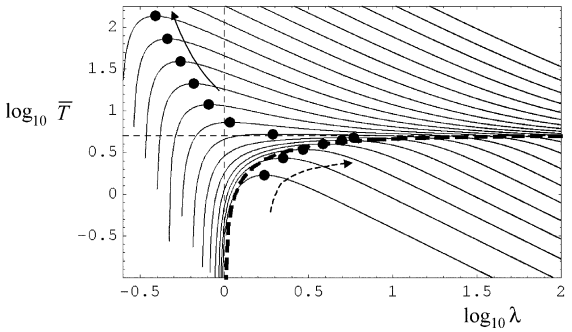

Fig. 2. Normalized true traction $\overline{T}$ at the outer surface as a function of the cavity stretch. Dashed line represents Green and Zerna's (1954) classical solution. For the set of curves marked by the dashed arrow, the dominating effect is the finite size of the shell; for the set of curves marked by the full arrow, the dominating effect is the constriction due to surface tension. (Arrows indicate the sense in which the cavity size decreases.)

less than $5E/6$ and it decreases with A/B. As $\overline{A}$ becomes smaller, the elastic response first approaches that of the thick spherical shell (8) as shown in Fig. 2. Subsequently, for $\overline{A} < 0.01$ surface tension increasingly constricts the cavity, i.e. one also finds $\lambda < 1$. The intersections of these curves with the vertical broken line $\lambda = 1$ give the level of true traction at which the collapsing effect of surface tension and the expanding effect of the applied load are equal, i.e. where there is no current deformation at the cavity surface while the stress and the deformation elsewhere are not necessarily zero. Thus, for sufficiently small cavities, as a result of surface tension, the true traction T can significantly exceed $5E/6$.

The problem with this description is that for vanishing initial cavity size, it predicts an infinite expansion stress. Experimentally, the values of cavitation stress that are measured are higher but not orders of magnitude larger than $5E/6$. We now explore an alternative method to study the same problem that leads to a potential explanation of the experimental results.

2. Energy analysis—mathematical frame work

The purpose of the present paper is to give more physical insight into expressions (2) and (7) and to obtain some understanding of the effect of surface tension in the context of cavity growth. This will be carried out as an analysis of potential energy rather than solving the field equations. Consider a material particle located at the coordinate $\vec{R}$ in the undeformed configuration. Its location in the deformed configuration is specified by the function $\vec{r}(\vec{R})$. The fundamental kinematic tensor underlying the local deformation in the vicinity of this particle is the deformation gradient tensor

$$\overleftrightarrow{F} = \frac{\partial \vec{r}}{\partial \vec{R}}. \tag{9}$$

2.1. Mapping function

Consider the elastic shell in Fig. 1. As a result of incompressibility, we have

$$R^3 - A^3 = r^3 - a^3. \tag{10}$$

Thus, the mapping function is given by

$$f(R) \equiv r(R) = (R^3 - A^3 + a^3)^{1/3} \tag{11}$$

for spherically symmetric deformations. Because of symmetry, the related stretch ratios λ_r, λ_θ, λ_ϕ are particularly simple:

$$\lambda_r = \mathrm{d}r/\mathrm{d}R, \tag{12}$$

$$\lambda_\theta = \lambda_\phi = r/R. \tag{13}$$

Locally, incompressibility may be expressed by

$$\lambda_r\lambda_\theta\lambda_\phi = 1. \tag{14}$$

2.2. Boundary conditions

On the external surface, $R = B$, there is a uniform distribution of radial outward tractions. In contrast with previous work (Green and Zerna, 1954; Ball, 1982), where a constant Cauchy traction is imposed at infinity, we assume that the total applied force is constant, or, equivalently, the nominal traction is constant. This type of loading is called *dead load*. The significance of using a dead loading instead of constant traction will be addressed in the discussion. It is easier to realize dead loading experimentally rather than have a uniform true traction on the external surface. During probe tack tests on soft adhesives, a rigid cylindrical flat-ended probe is pulled from the soft adhesive by prescribing a fixed displacement after establishing contact for a certain period of time. If we imagine the outer shell surface to be connected by linear springs to the rigid punch, the dead loading on the outer surface corresponds to the limiting case of zero spring stiffness. The total force F may therefore be expressed as

$$F = 4\pi B^2 P = 4\pi b^2 T, \tag{15}$$

where P, T denote the traction at the undeformed and deformed external surface respectively.

2.3. Potential energy

The principle of stationary potential energy is used in order to identify the equilibrium solutions of the system. The normalized potential energy Π^* (all energies are normalized by EA^3) is

$$\Pi^* = U^* + U^*_\gamma - W^*_{\mathrm{ext}}, \tag{16}$$

where

$$U^* = (4\pi/E)\int_1^{B/A} w(R', A, a)R'^2\,\mathrm{d}R' \tag{17}$$

is the normalized strain energy and the strain energy density w for the neo-Hookean material in terms of hoop stretch is

$$w(\lambda) = \frac{\mu}{2}\left[\frac{1}{\lambda^4} + 2\lambda^2 - 3\right]. \tag{18}$$

The normalized surface energy is

$$U^*_\gamma = 4\pi\alpha\lambda^2, \tag{19}$$

and

$$W^*_{\mathrm{ext}} = \frac{2\pi f^{-3}P^*}{3}\left[(1 + f^3(\lambda^3 - 1))^{1/3} - 1\right] \tag{20}$$

is the normalized external work due to the dead loading. The dimensionless parameters f, α and P^* are defined by

$$\alpha = \gamma/EA, \quad f = A/B, \quad P^* = 6P/E. \tag{21}$$

The equilibrium solution is obtained by enforcing the stationary condition

$$\mathrm{d}\Pi^*(\lambda)/\mathrm{d}\lambda|_{\lambda=\lambda^*} = 0. \tag{22}$$

This approach is different than the approach of Williams and Schapery (1965), where A is varied, and in accord with Ball (1982). The variational principle is used extensively in Hou (1990) to study cavity growth. There are three types of stationary solutions. If λ^* corresponds to a global minimum, the solutions is called *absolutely stable*, if it corresponds to a local minimum, it is called *meta-stable*, and if it corresponds to a maximum it is called *unstable*. It should be noted that the meta-stable solution always appears together with at least one unstable solution. This introduces the issue of bifurcation and activation energy, which will be discussed in Section 3.3. We identify the stationary solution over a range of normalized traction P^*.

3. Growth of a pre-existing cavity—two numerical examples

The undeformed exterior radius is taken to be $B = 50$ μm. We consider two numerical examples, $A = 10$ μm (surface tension forces not significant) and $A = 0.5$ μm (surface tension forces significant) i.e. $f = 0.2$ and 0.01 respectively.

3.1. Energy analysis for a large cavity ($f = 0.2$)

For large cavities, expressed by $\overline{A} > 1$ as discussed above, Gent and Tompkins (1969) predict the surface tension to be of negligible influence. This has been reviewed in connection with Fig. 2.

Fig. 3(a) and (b) plots the normalized potential energy Π^* against the cavity stretch $\lambda = a/A$ for different values of normalized nominal traction, P^* (see (21)). The full gray curve, in Fig. 3(a) represents Π^* in the absence of any externally applied load, $P^* = 0$. The dots indicate stationary solutions. The key feature is that, for any value of P^*, the energy curve has exactly one stationary point corresponding to a global minimum. In other words, at any applied nominal traction, the system is stable and there is no possibility of bifurcation. Let us inspect Π^* for low loads, Fig. 3(a). For $P^* = 0$, the global minimum corresponds to the deformed cavity radius $a|_{P^*=0} \approx 9.15$ μm. Since $A = 10$ μm, one recognizes that surface tension constricts an

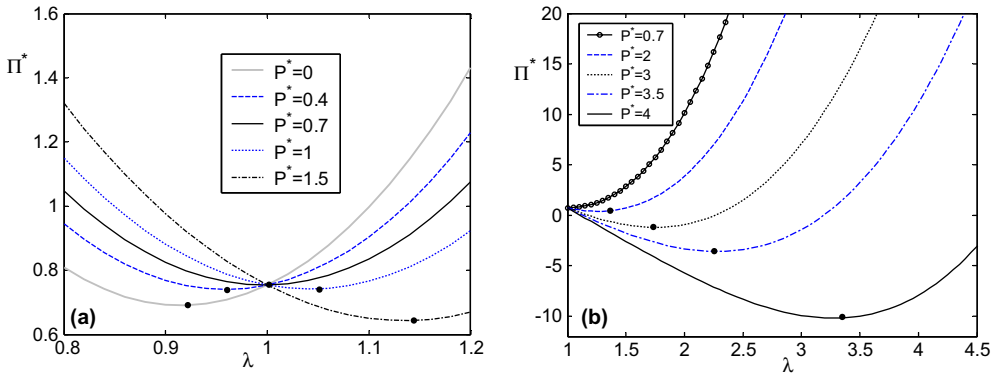

Fig. 3. Normalized potential energy plots for the large cavity case, $f = 0.2$ for different ranges of normalized nominal traction. Points indicate global minima.

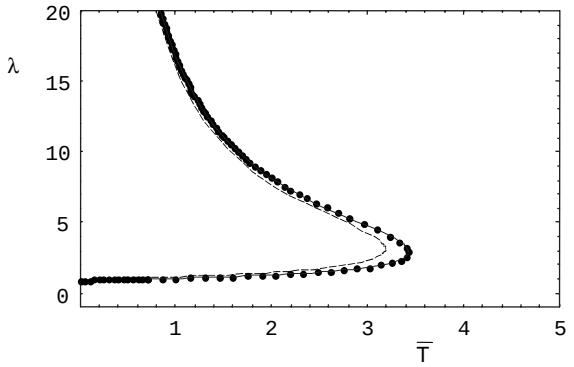

Fig. 4. Cavity stretch vs. normalized true traction $\overline{T}$. Points correspond to global minima of potential energy shown in Fig. 3. Drawn-out curve: analytical solution (7); dashed curve: analytical solution (7) without surface tension.

existing cavity. Next, at the comparatively weak load level of $P^* = 0.7$, the outward force due to the external load compensates exactly the inward force due to surface tension, $a|_{P^*=0.7} = A$. As the load further increases, cavity expansion finally sets in, which is shown in Fig. 3(b). The dots corresponding to the minima shown in Fig. 3 represent the solution of the finite-elasticity problem. In Fig. 4, the cavity stretch is plotted against the normalized true traction and is compared with the inversion of the corresponding analytical expression (7) with $T = P/\lambda_B^2$. One recognizes that the agreement is excellent.

3.2. Energy analysis for a small cavity ($f = 0.01$)

For such small cavities, expressed by $\overline{A} < 1$ as discussed above, Gent and Tompkins (1969) predict the surface tension effect to be significant and increase with decreasing cavity radius. For ease of later reference, three critical numbers found and frequently used in this section are introduced here and shown on Table 1.

Fig. 5(a)–(c) plots the normalized potential energy Π^* against the cavity stretch $\lambda = a/A$ for different values of normalized nominal traction. The square, triangle and star symbols correspond to stable, metastable and unstable states, respectively. Let us inspect Π^* for the range of *cavity constriction* (see Fig. 5(a)). The full gray curve indicates Π^* in the absence of any externally applied load, $P^* = 0$ and the minimum corresponds to a deformed cavity radius of $a|_{P^*=0} \approx 0.215$ μm. Comparing this to the undeformed radius, $A = 0.5$ μm, one recognizes that surface tension, as expected, constricts a smaller cavity more than the larger one studied previously in Section 3.1. As P^* increases, the radius of the compressed cavity gradually increases. Next, one recognizes that for $P^* > 15.25$ the minimum corresponding to cavity constriction completely disappears. Now consider Π^* for the range of *cavity expansion*, $a \geqslant A$, Fig. 5(b). For $P^* > P_1^*$, the function Π^* starts to develop a minimum at an $a \geqslant A$. The key feature distinguishing the present case from Section 3.1 is that for load levels $P_1^* \leqslant P^* \leqslant P_3^*$, the energy curve has two minima, not just one. One of these minima corresponds to cavity constriction, the other to cavity expansion. Obviously there is also a local maximum lying between each of the two minima, which corresponds to an unstable equilibrium solution. Let us now address the question which one of these minima is the global one. For $P^* \leqslant P_2^*$, the

Table 1
Critical values of normalized nominal traction for the small cavity case, $f = 0.01$

P_1^*	P_2^*	P_3^*
5.31	5.35	15.25

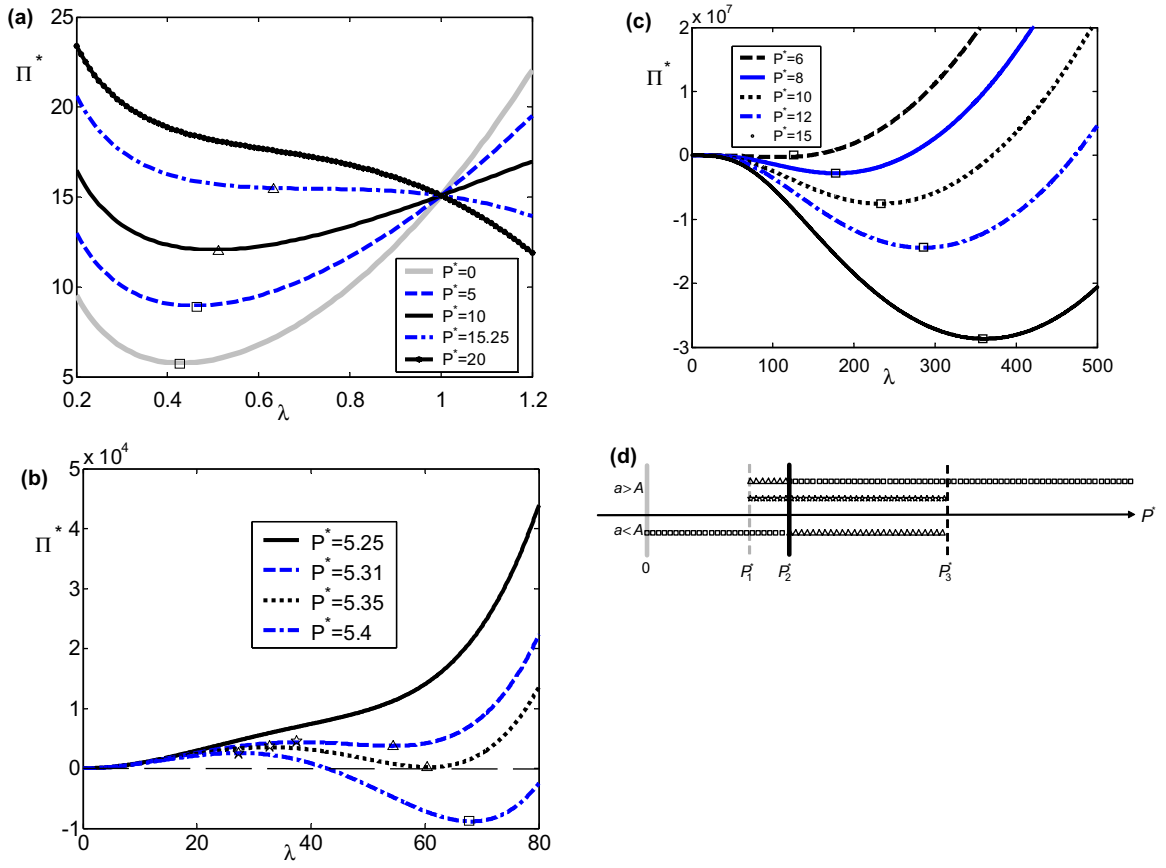

Fig. 5. Normalized potential energy plots for the small cavity case, $f = 0.01$. Boxes: global minima; triangles: local minima; stars: local maxima. (a) Regime of cavity constriction; (b) appearance of meta-stable expanded solutions; (c) regime of cavity expansion and (d) summary of equilibrium solutions.

minima corresponding to cavity constriction are energetically lower than those corresponding to cavity expansion. Hence, for $P^* \leqslant P_2^*$, cavity constriction is the stable and cavity expansion is the meta-stable equilibrium. Conversely, for $P^* > P_2^*$, cavity expansion is the stable and cavity constriction is the meta-stable equilibrium. For the sake of clarity, the loci of the equilibria are summarized in Fig. 5(d).

The equilibrium stretch on the cavity surface $\lambda(\overline{T})$ is plotted against the applied normalized Cauchy traction in Fig. 6. Points on this curve labeled by square, triangle and star symbols correspond to stable, meta-stable and unstable states respectively. These results agree well with the analytical expression (7). For comparison, the broken curve indicates the elastic response of the shell in the absence of surface tension, $\gamma = 0$. As expected, for the small cavity, surface tension enhances the maximum attainable Cauchy traction up to a factor of about 3. In addition, the results from the energy analysis give additional insight into the stability of the different branches of curves, which was not possible by directly solving the field equations.

3.3. Activation energy

In order to determine the growth of a cavity, one has to address the transition between meta-stable and absolutely stable states. One may rely either on the criterion of absolute stability or on the criterion of meta

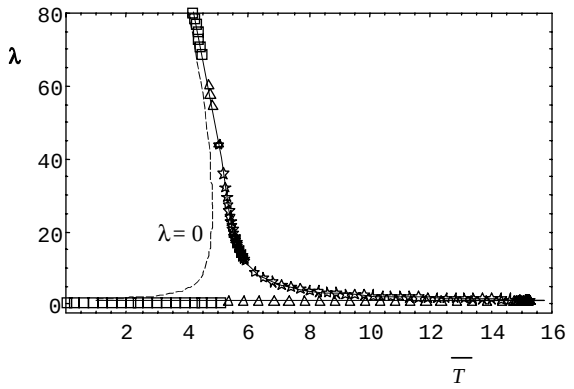

Fig. 6. Cavity stretch vs. normalized true traction $\overline{T}$. Boxes: global minima; triangles: local minima; stars: local maxima corresponding to the extrema of potential energy shown in Fig. 5. Drawn-out curve: analytical solution (7); dashed curve: analytical solution (7) without surface tension.

stability, the second of which will be used in this work. The first one stipulates that the system always remains in the *absolute minimum*. Then, if a load is applied to the system and gradually increased, the system will bifurcate from the compressed cavity equilibrium into the expanded cavity equilibrium when $P^* = P_2^*$, as is seen from Fig. 5(d). Alternatively, one can adopt the criterion of meta-stability. It stipulates that the system may be kept in a *local minimum* as long as the available activation energy, denoted by E_a, is not sufficient to make the system overcome the potential barrier separating the local from the global minimum. The activating energy E_a may be provided, for example, by a heat reservoir or by a reservoir of elastic energy. The principle of meta-stability is sketched in Fig. 7(a). The height of the *potential barrier* is denoted by E_c. The potential barrier corresponds to the difference between the local minimum of cavity constriction and the maximum corresponding to cavity expansion for each curve Π^*. If the elastic system is treated as a deterministic one, the only way to pass from the meta-stable compressed cavity into the stable expanded cavity is by attaining temporarily the unstable intermediate state corresponding to the maximum. This is possible if $E_a \geqslant E_c$. Otherwise, the constricted cavity configuration will persist until $P^* = P_3^*$. Alternatively, for describing a meta-stable system, a more advanced, probabilistic approach could be adopted. From Fig. 7(b), it can be seen that the potential barrier $E_c(P^*)$ decreases with increasing P^*. For a given P^*, this barrier is defined as the difference in potential energy

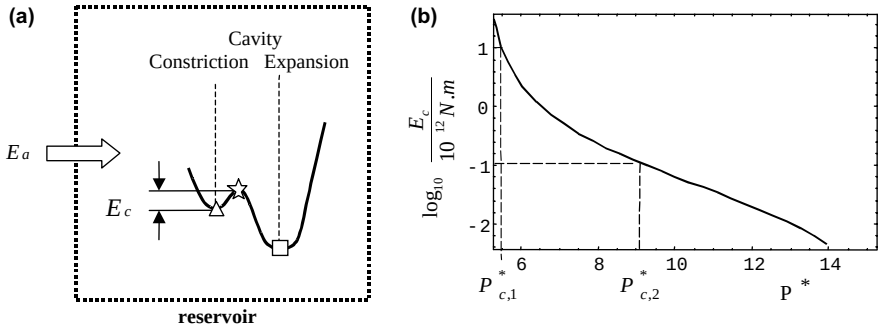

Fig. 7. Activation energy issue (a) activation energy barrier E_c and available activating energy E_a. (b) Variation of activation energy barrier with normalized nominal traction.

$$E_c(P^*) \equiv \Pi(a_u)|_{P^*} - \Pi(a_m)|_{P^*}, \tag{23}$$

where $a_m < A, a_u > A$ denote the deformed equilibrium radii of the constricted meta-stable and the expanded unstable solution, respectively. $E_c(P^*)$ can be obtained using (16) and (23) and is shown in Fig. 7(b). Recall that the barrier disappears when $P^* = P_3^*$.

As an example, consider the values $E_{c,1} = 10^{-11}$ N m and $E_{c,2} = 10^{-13}$ N m (taken ad hoc and without reference to any thermodynamic description). Assume that there is as much activation energy as $E_{a,1} = 10^{-11}$ N m. Then, the initially constricted cavity instantly expands since $E_{a,1} = E_{c,1}$. Fig. 7(b) tells that this will happen at the nominal stress $P_{c,1}^* \equiv 5.5$. Repeating the same arguments for the case where the available activating energy is $E_{a,2} = 10^{-13}$ N m one finds a critical stress of $P_{c,2}^* \equiv 9.1$ is necessary to trigger the transition. Similar discontinuous transitions were also obtained for cavitation in incompressible anisotropic elastic spheres (Polignone and Horgan, 1993), for composite isotropic incompressible spheres (Horgan and Pence, 1989a,b) and for compressible anisotropic spheres and cylinders (Antman and Negrón-Marrero, 1987). Such behavior was called *snap cavitation* by analogy with the snap-through buckling phenomenon of structural mechanics.

3.4. Rate of cavity expansion

Instead of plotting $\lambda(\overline{T})$, one may express the numerical result in terms of the function $a(P^*)$ giving the dependence of the deformed cavity radius upon the normalized nominal traction. It is to be noted that P^* is proportional to the applied total force through (15). This will allow us to compare these results with experimental data on cavitation in adhesives. Typically, applying an increasing load to a thin confined layer triggers cavitation in soft adhesives. Since the adhesive is linear elastic for small deformations, the applied load on the layer increases linearly with time as long as one restricts attention to the appearance of the first few cavities in the thin film (the appearance of the first cavities does not considerably affect the slope of the load-displacement curve, Chiche et al., 2003).

Consequently, up to a rescaling of the P^*-axis, $a(P^*)$ corresponds to a curve $a(t)$ giving the evolution of the cavity radius with time. Consider Fig. 8 showing $a(P^*)$ for the large cavity of Section 3.1 (symbols: dots) and the small cavity of Section 3.2 (symbols as in Fig. 5(d)). For the large cavity, growth is continuous. Roughly, the growth rate $\dot{a} \equiv \frac{da(t)}{dt}$ is weak and more or less constant up to $P^* \approx 3.5$ and then accelerates by a factor of about 3. For the small cavity, let us assume the criterion of meta-stability introduced in Section

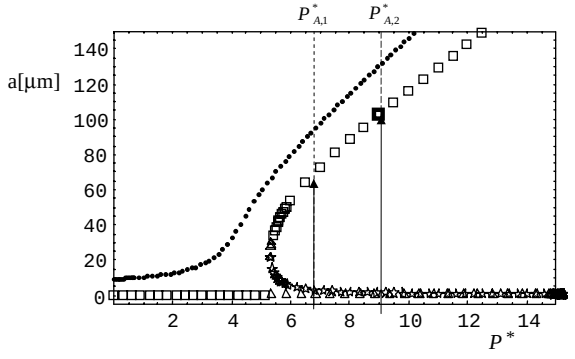

Fig. 8. Deformed cavity radius vs. normalized nominal traction P^*. Boxes: global minima; triangles: local minima; stars: local maxima, corresponding to the extrema of potential energy shown in Fig. 5 for small cavity case. Points represent global minima of potential energy shown in Fig. 3 for large cavity case. Arrows: bifurcations from the meta-stable cavity constriction into the absolutely stable cavity expansion.

3.3. Consider two cases of available activation energy $E_{a,1} = 10^{-11}$ N m and $E_{a,2} = 10^{-13}$ N m. The snap expansions will occur as indicated by the arrows at $P^*_{A,1}$ and $P^*_{A,2}$ respectively. In a perfectly elastic setting, this will give rise to an infinite cavity growth rate. In a realistic setting with dissipation, these instant snaps will be somewhat smeared out and be observed as fast cavity growth (Chiche et al., 2003). Consequently, the conclusions for the small initial cavity are as follows: In the first case, the cavity barely grows (cf. Fig. 6) until $P^* = 6.8$ is reached. Then, it will grow very fast until it reaches a cavity radius of about 70 μm (for comparison, note that the large initial cavity, at this load, has grown to about 90 μm). In the second case, the cavity hardly grows until $P^* = 9.1$ is reached. Then, it will grow very fast until it reaches a cavity radius of about 100 μm (for comparison, note that the large initial cavity, at this load, has grown to about 110 μm). After the snap, in both cases, cavity growth continues at about the same rate.

Next, consider the time evolution $a(t)$ of the cavity radius, as found in typical probe tack experiments. The force applied to the adhesive layer increases linearly with time. The evolution displayed in Fig. 9(a) has been obtained from a series of images showing, in situ, the PSA/glass interface during the loading process (Chiche et al., 2003). Two typical still pictures are given in Fig. 9(b). It appears that a number of cavities appear at very low load levels (such as cavity "a" in Fig. 9(b) which appears at 0.1 MPa corresponding to $P^* = 3$). This type of cavity grows steadily as shown on Fig. 9(a). In addition, another type of cavity expansion is observed, optically appearing at much higher stress and growing much more rapidly than the cavity originating from visible precursors (the cavity "b" in Fig. 9(b) is an example). In order to confront experiment and model predictions, now let us compare the snap transition predicted by the first arrow on Fig. 8, and the experimental result of Fig. 9(a). In the early stages of the test, $\overline{P} \propto t$ so that the two figures can be qualitatively compared.

Consider cavity "*b*" in Fig. 9(a). For times $t < 7$ s, no precursor could be identified optically (Chiche et al., 2003). In the interval 7 s $< t <$ 8 s, this cavity rapidly grows up to about 80% of the size reached by the cavity "*a*" at the same load. Qualitatively, this is very close to what is predicted by the model for the

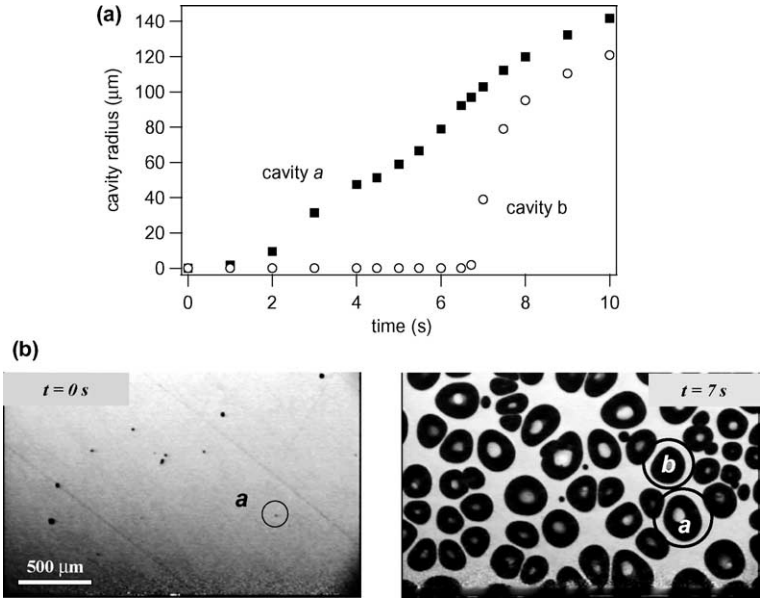

Fig. 9. In situ observation of cavity growth taken with the video probe tack set-up. (a) Cavity radius in projection as a function of time during a probe test for the two different cavities shown on (b). (b) Snap-shots of the interface between the probe and the adhesive film at $t = 0$ s (corresponding to $P^* = 3$) and at $t = 7$ s (corresponding to $P^* \sim 19$).

snap expansion occurring at $\overline{P}_c = 6.8$ corresponding to an available activation energy of $E_a \approx 10^{-12}$ N m. The model predicts the small cavity studied in Section 3.2 to snap open to about 75% of the size reached by the large cavity at the same load.

Of course, one might object that we compare results obtained from a model for a homogenous material to experiments, which seem to give evidence of an interfacial debonding process. However it is important to note that if the initial nucleation of the cavity occurs at or near the interface, its expansion is clearly in the bulk of the soft material and we do not have much evidence of extensive interfacial debonding. While, at present, it seems too early to correctly model the interfacial aspect of the experiment, we feel that the physics of the different growth rate of the cavities is well captured by the notion of transition from a metastable to a stable state. Furthermore this picture of cavity growth is qualitatively consistent with experimental observations mentioned in the beginning of the paper, i.e. the fact that cavities can expand rapidly after a certain time under stress and that cavities expand at higher level of stress when the layer is thinner (i.e. for the same applied stress, less elastic energy is available to overcome the activation barrier).

4. Cavity nucleation

The same formulation can be used to study cavity nucleation in an initially solid sphere. For the case of a pre-existing cavity, λ is well defined since $A \neq 0$ For an initially solid sphere, $A = 0$, and we cannot use the same normalization. The potential energy Π is

$$\Pi = U + U_\gamma - W_{\text{ext}}, \tag{24}$$

where

$$U = 4\pi \int_0^B w(R', a) R'^2 \, \mathrm{d}R' \tag{25}$$

is the strain energy. The surface energy is

$$U_\gamma = 4\pi\gamma a^2 \tag{26}$$

and

$$W_{\text{ext}} = 4\pi B^2 P(b - B) \tag{27}$$

is the external work due to the dead loading. As before, we determined the equilibrium solution by finding the stationary points of the potential energy function. For the case of $B = 50$ μm, our analysis shows that for nominal traction $P \leqslant 0.9E$, there exists only one solution, which corresponds to the global minimum of potential energy. Hence, for nominal traction smaller than $0.9E$, the solid (uncavitated) configuration is absolutely stable. Note that, for $\gamma = 0$, from Ball (1982), cavity nucleation occurs at $P = 5E/6$ whereas in our case, the nucleation stress is higher due to surface tension and finite shell effects. For applied nominal stresses $P > 0.9E$, the potential energy curve develops a second minimum at a finite deformed cavity radius corresponding to a cavity nucleating in the sphere. As long as $0.9E < P \leqslant 0.91E$, the second stationary point is a local minimum and the potential energy of the solid configuration is still the absolute minimum. For $P > 0.91E$, the stationary points corresponding to the finite deformed cavity radius becomes the global minimum, so that the cavitated configuration is absolutely stable.

The nucleated cavity has a radius $a = 27$ μm at $P = 0.9E$, for our choice of material parameters mentioned previously. The nucleated cavity continues to grow as the load increases and the growth with the normalized Cauchy traction $\overline{T}$ is plotted in Fig. 10. Apart from the normalization with an undeformed cavity radius A which is not available for the initially solid configuration, the behavior of $a(\overline{T})$ in Fig. 10 is analogous to Fig. 6. The solid line shows Ball's classical result (no surface tension). The two broken lines

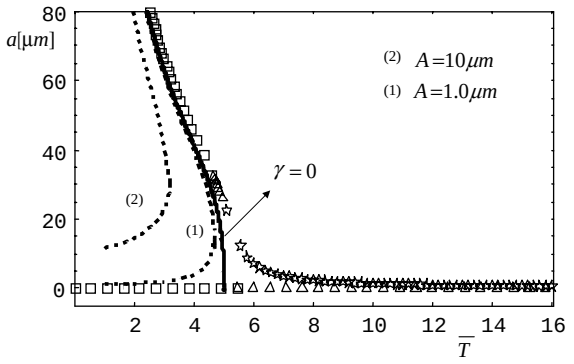

Fig. 10. Deformed cavity radius a vs. normalized true traction $\overline{T}$. Boxes: global minima; triangles: local minima; stars: local maxima corresponding to the extrema of potential energy; drawn-out curve: Ball's (1982) classical solution; broken curves: solution for growth of pre-existing cavities without surface tension.

show (no surface tension) the relationship $a(\overline{T})$ for two cases of a pre-existing cavity with undeformed cavity sizes 1 and 10 μm.

5. Summary and outlook

The role of surface tension was first considered by Gent and Tompkins (1969) under constant traction conditions and for an infinite specimen, only one stable solution is observed under these assumptions. In this work, the effect of surface tension on cavity growth in an incompressible neo-Hookean material (finite size specimen) under dead loading was examined and multiple solutions were obtained for certain parameter sets. In a numerical analysis of potential energy limited to spherically symmetric configurations, a bifurcation problem is identified. If the applied uniform radial tensile dead-load is sufficiently large, a branch corresponding to cavity expansion bifurcates from the branch corresponding to cavity constriction due to of surface tension. The bifurcation is interpreted in terms of a sudden growth to a finite cavity radius which bears some reminiscence of the snap-through buckling phenomenon in structural mechanics. The finding is compared to experimental results obtained in probe tack tests of soft adhesives where rapid cavity growth is also observed and we obtained good agreement with our model. The formulation of the problem in those terms suggests that the growth of a small cavity in a soft material could be an energy activated process, in agreement with experimental results obtained on soft adhesives.

In order to simulate more accurately experimental results, several improvements of the model can be envisioned. First of all a detailed finite element simulation might be able to tackle the growth of a cavity at the interface between a rigid material and the soft rubber, then a different type of strain energy function than the neo-Hookean one could be used to provide a better representation of the nonlinear elastic properties of the adhesive. Finally, the role of viscoelasticity needs to be investigated to better understand the cavitation process (Brown and Creton, 2002).

Equilibrium solutions were also found by solving all the field equations and we obtained the same results as the energy approach outlined above. Such a method based on solving the field equations is particularly well suited when we extend the above analysis to model viscoelastic effects.

Finally, we have also extended our model to account for finite compliance effects (not discussed here) and similar results were observed i.e. multiple solutions were found for some parameter sets. These results and the effects of material hardening will be presented in an upcoming paper.

Acknowledgements

The present research was carried out with the financial support of the European research programme GROWTH: contract no. G5RD-CT-2000-00202 DEFSAM, which is gratefully acknowledged. The authors also thank Prof. Manuel Laso, ETSII/UPM, Madrid, for helpful discussions.

Appendix A

A.1. Formulation

A homogeneous, isotropic, incompressible elastic material is characterized by its elastic potential $W(\lambda_1, \lambda_2, \lambda_3)$ where the λ_i's denote the principal stretches associated with the deformation and $\lambda_1\lambda_2\lambda_3 = 1$.

The principal values of the Cauchy stress tensor is given by

$$\tau_i = \lambda_i W_i - p, \tag{A.1}$$

where $W_i = \partial W/\partial\lambda_i$ and the pressure term p arises because of the incompressibility constraint. Here, we are concerned with isochoric deformations in which two of the principal stretches coincide: $\lambda_2 = \lambda_3$. Hence, it is convenient to define a function w by

$$w(\lambda) = W(\lambda^{-2}, \lambda, \lambda) \quad \text{for } \lambda > 0, \tag{A.2}$$

which is the restriction of W to such deformations. We assume that w is twice continuously differentiable on its domain of definition and that $w(1) = w'(1) = 0$. From (A.1) and (A.2), we get

$$\tau_1 = \lambda^{-2} W_1(\lambda^{-2}, \lambda, \lambda) - p, \quad \tau_2 = \tau_3 = \lambda W_2(\lambda^{-2}, \lambda, \lambda) - p, \tag{A.3}$$

where $\lambda = \lambda_2$; thus,

$$\tau_1 - \tau_2 = \tau_1 - \tau_3 = -\frac{\lambda}{2} w'(\lambda). \tag{A.4}$$

Finally, note that the Baker–Ericksen inequality $(\tau_1 - \tau_2)(\lambda_1 - \lambda_2) > 0$ for $\lambda_1 \neq \lambda_2$ requires that

$$(\lambda - 1)w'(\lambda) > 0 \quad \text{for } \lambda > 0, \ \lambda \neq 1. \tag{A.5}$$

In the reference configuration, the body occupies a region Ω exterior to the cavity of radius A. The radial and hoop stretches associated with the radial deformation are

$$\lambda_r = r'(R), \quad \lambda_\theta = \lambda_\phi = r(R)/R, \tag{A.6}$$

where the particle at R is carried to r as a result of the deformation. Finally, since the material is incompressible,

$$r(R) = (R^3 + a^3 - A^3)^{1/3}, \tag{A.7}$$

where A and a represent the cavity radius in the reference and current configurations respectively. The boundary conditions are as follows.

A uniform tension T is applied at infinity,

$$\lim_{R\to\infty} \tau_r(R) = T, \tag{A.8}$$

whereas at the cavity because of the surface tension forces, we have

$$\tau_r(A) = \frac{2\gamma}{a} \quad \text{and} \quad a > 0. \tag{A.9}$$

The radial and hoop components of Cauchy stress τ_r and τ_θ are given by (A.3) with $\tau_r = \tau_1$, $\tau_\theta = \tau_2$ and $\lambda = \lambda_\theta$. By virtue of (A.6), the radial equilibrium equation

$$\frac{\mathrm{d}\tau_r}{\mathrm{d}r} + \frac{2}{r}(\tau_r - \tau_\theta) = 0 \tag{A.10}$$

can be written as

$$\frac{\mathrm{d}\tau_r}{\mathrm{d}R} + \frac{2\lambda_r}{R\lambda_\theta}(\tau_r - \tau_\theta) = 0. \tag{A.11}$$

Substituting (A.4) into (A.11), integrating the resulting equation from R to ∞, using the boundary condition (A.8), and finally changing the variable of integration from R to λ_θ by using (A.6) and (A.7), yields the following expression for the radial component of Cauchy stress

$$\tau_r(R) = T + \int_\lambda^1 \frac{w'(\lambda')}{\lambda'^3 - 1}\,\mathrm{d}\lambda', \tag{A.12}$$

$$\lambda_\theta = \left[1 + \frac{a^3 - A^3}{R^3}\right]^{1/3}. \tag{A.13}$$

Applying the boundary condition (A.9), we get

$$\frac{2\gamma}{a} = T + \int_{a/A}^1 \frac{w'(\lambda')}{\lambda'^3 - 1}\,\mathrm{d}\lambda'. \tag{A.14}$$

The problem at hand is thus reduced to the following: Given the initial cavity size A, the surface energy γ and the material properties, we are interested in finding the deformed cavity size a and whether the deformed configuration is stable or not.

A.2. Exact analysis for neo-Hookean case

We now carry out an exact analysis of the problem for the neo-Hookean case. Here, the strain energy function is given by

$$W = \frac{\mu}{2}\left[\frac{1}{\lambda^4} + 2\lambda^2 - 3\right] \tag{A.15}$$

with μ being the infinitesimal shear modulus. Hence, the integrand of (A.14) simplifies to

$$\frac{w'(\lambda)}{\lambda^3 - 1} = \frac{1}{\lambda^2} + \frac{1}{\lambda^5}. \tag{A.16}$$

A.2.1. No surface forces

We first consider the case with no surface forces first to see the effect of the tension at infinity alone of the cavity growth. So, (A.14) simplifies to

$$-T = \int_{\lambda}^{1} 2\mu\left(\frac{1}{\lambda'^2} + \frac{1}{\lambda'^5}\right) \mathrm{d}\lambda' \tag{A.17}$$

or,

$$\frac{-T}{2\mu} = \frac{1}{\lambda} + \frac{1}{4\lambda^4} - \frac{5}{4}. \tag{A.18}$$

The above equation predicts that, beyond a critical tension T_c, given by 2.5μ, no equilibrium solution exists and the cavity will expand without limit.

A.2.2. With surface forces

We consider the effect of including the surface forces too in the model for cavity growth. For this case, (A.14) simplifies to

$$\frac{-T}{2\mu} + \frac{\gamma}{A\mu}\frac{1}{\lambda} = \frac{1}{\lambda} + \frac{1}{4\lambda^4} - \frac{5}{4}. \tag{A.19}$$

A.2.3. Finite shell size

When the outer shell radius is finite, then (A.14) becomes

$$\frac{2\gamma}{a} = T + \int_{a/A}^{\lambda_B} \frac{w'(\lambda')}{\lambda'^3 - 1} \mathrm{d}\lambda', \tag{A.20}$$

which then simplifies to (for a neo-Hookean model):

$$\frac{-T}{2\mu} + \frac{\gamma}{A\mu}\frac{1}{\lambda} = \frac{1}{\lambda} + \frac{1}{4\lambda^4} - \frac{1}{\lambda_B} - \frac{1}{4\lambda_B^4}. \tag{A.21}$$

References

Abeyratne, R., Hou, H.S., 1991. Void collapse in an elastic solid. J. Elasticity 26, 23–42.

Antman, S.S., Negrón-Marrero, P.V., 1987. The remarkable nature of radially symmetric equilibrium states of aeolotropic nonlinearly elastic bodies. J. Elasticity 18, 131–164.

Ball, J.M., 1982. Discontinuous equilibrium solutions and cavitation in nonlinear elasticity. J. Philos. Trans. Roy. Soc. Lond. A 306, 557–611.

Brown, K., Hooker, J.C., Creton, C., 2002. Micromechanisms of tack of soft adhesives based on styrenic block copolymers. Macromol. Mater. Eng. 287, 163–179.

Brown, K.R., Creton, C., 2002. Nucleation and Growth of cavities in soft viscoelastic layers under tensile stress. Eur. Phys. J. Eng. 9, 35–40.

Chiche, A., Dollhofer, J., Creton C., 2003. Available from <http://hal.ccsd.cnrs.fr/>. ccsd-00001473; Chiche A. Ph.D. Thesis, Université Paris VI.

Gent, A.N., Tompkins, D.A., 1969. Surface energy effects for small holes or particles in elastomers. J. Polym. Sci. Part A2 7, 1483–1488.

Green, A.E., Zerna, W., 1954. Theoretical Elasticity. Clarendon Press, Oxford.

Horgan, C.O., Pence, T.J., 1989a. Void nucleation in tensile dead-loading of composite incompressible non-linearly elastic sphere. J. Elasticity 21, 61–82.

Horgan, C.O., Pence, T.J., 1989b. Cavity formation at the centre of a composite incompressible non-linearly elastic sphere. J. Appl. Mech. 56, 302–308.

Hou, H.-S., 1990. Cavitation instability in solids. Ph.D. Thesis. Massachusetts Institute of Technology.

Lakrout, H., Sergot, P., Creton, C., 1999. Direct observation of cavitation and fibrillation in a probe tack experiment on model pressure-sensitive-adhesives. J. Adhes. 69, 307–359.

Polignone, D.A., Horgan, C., 1993. Cavitation for incompressible anisotropic nonlinearly elastic spheres. J. Elasticity 33, 27–65.

Williams, M.L., Schapery, R.A., 1965. Spherical flaw instability in hydrostatic tension. Int. J. Fract. Mech. 1, 64–71.